Phytochemical-driven antibiofilm effects of *Ruellia tuberosa* L. against *Escherichia coli* and *Klebsiella pneumoniae*

ANURANJINI CHARACKAL[1], ARUN BASKARAPILLAI[2] and GEETHA ROYAPURAM VEERARAGAVAN[3]

[1]Department of Medical Microbiology, AKG Co-Operative Institute of Health Sciences (AKG CIHS), Mavilayi, Kannur, Kerala 670622, India; [2]Department of Biotechnology and Microbiology, Janakiammal Campus, Kannur University, Kannur, Kerala 670002, India; [3]Department of Microbiology, Centre for Infectious Diseases, Saveetha Dental College and Hospitals, Saveetha Institute of Medical and Technical Sciences (SIMATS), Saveetha University (Deemed to be University), Chennai, Tamil Nadu 600077, India

Received December 24, 2025; Accepted March 17, 2026

DOI: 10.3892/wasj.2026.457

Abstract. Multidrug-resistant Gram-negative pathogens, including *Escherichia coli* (*E. coli*) and *Klebsiella pneumoniae* (*K. pneumoniae*) represent major clinical concerns due to their potent biofilm-forming ability and associated virulence traits that contribute to persistent infections and antibiotic failure. In response to the growing limitations of conventional antibiotics against biofilm-associated infections, the present study evaluated the antibiofilm potential of the ethanolic leaf extract of *Ruellia tuberosa* L. (*R. tuberosa* L.) using *in vitro* assays and gas chromatography-mass spectrometry-guided molecular docking analysis. The extract demonstrated antibacterial activity at the minimum inhibitory concentration (MIC) level and effectively inhibited biofilm formation at sub-MIC concentrations, achieving 55% inhibition in *E. coli* at 10 mg/ml and 67.81% inhibition in *K. pneumoniae* at 20 mg/ml, without significantly affecting planktonic growth. Phytochemical profiling revealed a diverse compound composition, with diethyl phthalate identified as the major constituent. Molecular docking demonstrated stable interactions of this compound with key biofilm- and virulence-associated targets in both pathogens, suggesting interference with bacterial adhesion, biofilm development, and persistence. Overall, these findings highlight *R. tuberosa* L. as a promising natural source of antibiofilm agents capable of attenuating biofilm formation in multidrug-resistan Gram-negative pathogens. These plant-derived compound may serve as adjunct strategies for managing biofilm-associated infections caused by *E. coli* and *K. pneumoniae*, warranting further *in vivo* and molecular validation.

Correspondence to: Dr Geetha Royapuram Veeraragavan, Department of Microbiology, Centre for Infectious Diseases, Saveetha Dental College and Hospitals, Saveetha Institute of Medical and Technical Sciences (SIMATS), Saveetha University (Deemed to be University), 162 Poonamallee High Road, Chennai, Tamil Nadu 600077, India
E-mail: rvgeetha2015@gmail.com

Key words: Escherichia coli, Klebsiella pneumoniae, Ruellia tuberosa L, biofilm, diethyl phthalate

Introduction

Bacterial biofilms consist of organized populations of microorganisms embedded within a self-produced extracellular polymeric matrix (EPS), enabling surface attachment and conferring substantial resistance to antimicrobial agents and host immune defense (1). As biofilm-embedded cells are markedly more tolerant than their planktonic counterparts, they play a central role in persistent, recurrent and device-associated infections, rendering effective biofilm control a major clinical priority (1,2). Among these pathogens, Gram-negative bacteria characterized by their lipopolysaccharide rich outer membrane and intrinsic resistance mechanisms are particularly challenging (3). Notably, *Escherichia coli* (*E. coli*) and *Klebsiella pneumoniae* (*K. pneumoniae*) are key Gram-negative species commonly associated with infections of the urinary tract, respiratory system, bloodstream and indwelling medical devices, particularly among hospitalized or immunocompromised individuals. Their strong ability to adhere to host tissues and medical devices, combined with robust biofilm formation, enables persistent colonization and substantially hinders eradication with conventional antibiotic therapies (4-6).

In the present study, *E. coli* and *K. pneumoniae* were selected as representative Gram-negative pathogens due to their clinical prevalence, strong biofilm-forming capacity and reliance on well-characterized virulence and quorum sensing (QS) regulated adhesion mechanisms. *E. coli* encompasses diverse pathogenic pathotypes that employ a variety of virulence factors, including fimbrial adhesins (such as type 1 fimbriae), curli fibers (CsgA fibrils), toxins, iron acquisition systems and secretion systems, to adhere to host tissues and evade immune defenses. Curli fibers, composed primarily of CsgA subunits, are major components of the extracellular matrix and show a critical role in surface adhesion, cell-cell aggregation, and biofilm stability. Similarly, the *E. coli* common pilus (ECP), assembled with the aid of the chaperone

EcpB, contributes to initial attachment and biofilm maturation on both biotic and abiotic surfaces (7-10). Biofilm development in *E. coli* progresses through stages of initial adhesion, microcolony formation, maturation and dispersion, and is tightly regulated by global transcriptional regulators and QS systems. The QS network, involving signaling molecules, such as autoinducer-2 and indole, coordinates the expression of genes controlling curli and pili production, biofilm formation, motility and antibiotic tolerance in a cell-density-dependent manner (8).

K. pneumoniae is a capsulated Gram-negative pathogen of major clinical concern, selected in the present study due to its potent biofilm-forming ability, extensive virulence repertoire and global association with multidrug resistance (MDR) (11). Among these, the type 3 fimbrial subunit MrkA serves as a critical structural component of type 3 fimbriae, mediating attachment to host tissues and medical devices and playing a central role in biofilm initiation, maturation and stability. QS systems in *K. pneumonia* can control the production of fimbriae, EPS and other virulence-associated factors in response to AI accumulation. QS regulators, such as SdiA coordinate fimbriae expression, biofilm development, and signal molecule production, emphasizing the importance of cell-cell communication in pathogenicity (12,13). In addition, *K. pneumoniae* is a major reservoir of antibiotic resistance determinants, most notably New Delhi metallo-β-lactamase-1, which confers resistance to carbapenems and other β-lactam antibiotics. The coexistence of robust biofilm formation and MDR significantly complicates treatment, rendering *K. pneumoniae* a critical threat in healthcare settings and a driver of the global spread of MDR infections (14).

In the current clinical landscape, conventional antibiotics frequently fail to eradicate biofilm-associated infections due to restricted penetration through the EPS matrix, the diminished metabolic activity of sessile cells, and the persistence of highly tolerant subpopulations. In addition, biofilm-embedded persister cells exhibit metabolic dormancy and upregulated efflux mechanisms, further compromising therapeutic efficacy in clinical conditions, such as catheter-associated urinary tract infections (CAUTIs) and ventilator-associated pneumonia (VAP) (7,15,16). Collectively, the well-characterized biofilm architectures, QS-regulated virulence systems, and MDR profiles of *E. coli* and *K. pneumoniae* render them highly relevant models for evaluating antibiofilm and anti-virulence strategies. These challenges underscore an escalating clinical crisis and highlight the urgent need for alternative therapeutic approaches that move beyond conventional bactericidal paradigms, focusing instead on disrupting biofilm formation and virulence regulation while minimizing selective pressure for resistance development.

Medicinal plants represent a valuable source of structurally diverse natural compounds that exhibit well-documented antimicrobial, antibiofilm and anti-virulence properties. Notably, these plant-derived molecules often exhibit fewer side-effects compared to conventional antibiotics, rendering them promising alternatives for managing resistant infections (17-19). Plant-derived phytochemicals, including flavonoids, phenolic acids, terpenoids, alkaloids and essential oils, have been widely reported to interfere with QS signaling, inhibit biofilm formation and suppress the expression of virulence factors in Gram-negative pathogens, frequently at sub-minimum inhibitory concentration (MIC) concentrations (20-22). Among these, *Ruellia tuberosa* L. (*R. tuberosa* L) is a medicinal plant traditionally recognized for its diverse pharmacological properties, including anti-inflammatory, antioxidant and antimicrobial activities. Previous antimicrobial studies on *R. tuberosa* L. have largely reported modest antibacterial activity, often requiring high extract concentrations to achieve growth inhibition (23-26). Amajida *et al* (26) observed antibacterial effects against *E. coli* only at concentrations as high as 500 mg/ml, indicating bactericidal potency under conventional MIC-based screening conditions. The discrepancy in potency may be attributed to differences in extract preparation, bacterial strains tested, and the use of growth inhibition endpoints rather than biofilm-specific or anti-virulence assays (23-26). In addition, the present study demonstrates significant antibiofilm inhibition at substantially lower, sub-MIC levels, suggesting a mechanism that selectively attenuates virulence without affecting bacterial growth. This mechanistic divergence from conventional bactericidal approaches reinforces the novelty of the present findings.

Although several medicinal plants have been evaluated for antimicrobial properties (20), studies that systematically integrate sub-MIC antibiofilm evaluation, QS-related virulence targeting, phytochemical profiling, and *in silico* mechanistic prediction against clinically relevant *E. coli* and *K. pneumoniae* biofilm-forming pathogens remain limited. The novelty of the present study lies in demonstrating the growth-neutral antibiofilm activity of *R. tuberosa* extract at sub-MIC level against MDR *E. coli* and *K. pneumoniae*, combined with gas chromatography-mass spectrometry (GC-MS)-guided molecular docking to predict interactions with key adhesion and virulence-associated proteins. This integrated experimental computational approach provides mechanistic insight into anti-virulence activity beyond conventional bactericidal screening.

Materials and methods

Isolates and growth conditions. The present study included two MDR clinical isolates: One *E. coli* isolate obtained from a urinary tract infection and one *K. pneumoniae* isolate obtained from a respiratory tract specimen. The bacterial isolates used in the present study were provided as a laboratory gift from the Department of Microbiology, Saveetha Dental College and Hospitals, Chennai, India, at an earlier time and were subsequently transferred to Kannur University, Kerala, for research purposes. The isolates were obtained from the hospital and were transferred by the laboratory authorities to the Kannur University laboratory for research use. The present study did not involve direct patient interaction, access to patient records, or collection of clinical specimens. The isolates were handled strictly as microbiological strains for *in vitro* experimental purposes. Upon receipt, the isolates were reconfirmed in the laboratory based on standard morphological characteristics prior to experimental use. As the study involved only de-identified bacterial isolates and did not include human participants or identifiable patient data, ethics approval and informed patient consent were waived. The cultures were maintained under aerobic conditions at 37˚C in brain heart infusion (BHI)

broth (HiMedia Laboratories). Prior to the experimental assays, the isolates were sub-cultured to the logarithmic phase to ensure optimal growth and viability. Isolates identities were confirmed using the automated VITEK® 2 system (BioMérieux, Inc.) for precise microbial identification. The results were further validated using the standardized identification keys described in Bergey's Manual of Determinative Bacteriology (27), along with the assessment of characteristic colony morphology and growth patterns on MacConkey agar.

Collection of plant material. Fresh leaves of *R. tuberosa* L. were collected from the Velappanchavadi area, Chennai, Tamil Nadu, India. The plant material (leaves) was authenticated by a qualified botanist prior to further solvent extract processing.

Preparation and preliminary screening of R. tuberosa L. The harvested leaves were rinsed three times with distilled water to eliminate adhering debris and surface impurities. Following surface sterilization, the leaves were shade-dried at room temperature and was then pulverized into a coarse powder using a mechanical grinder. For extraction, 50 g of the powdered leaves were soaked in 150 ml ethanol (Rankem Laboratories, LLC, India) and incubated in a shaking incubator at 150 rpm and 37˚C for 4 days. The resulting extract was filtered using Whatman filter paper (HiMedia Laboratories) after 4 days to obtain a clear filtrate (Fig. 1). The dried material was weighed and stored at 4˚C for subsequent use.

Antibiogram profiling and antimicrobial screening of R. tuberosa L. Antibiogram profiling was followed by the disk diffusion method as per the Clinical and Laboratory Standards Institute (CLSI) 2022 guidelines (28). A $1.5x10^8$ CFU/ml (0.5 McFarland standard) inoculum was uniformly spread across Mueller-Hinton agar (MHA) plates (HiMedia Laboratories) with a sterile swab, antibiotic discs placed following brief drying, and plates incubated at 37˚C for a day. The antibiotics evaluated included ampicillin, ceftriaxone, ciprofloxacin, gentamicin, imipenem and colistin (HiMedia Laboratories Private Limited). Zone diameters were measured post-incubation and categorized as susceptible or resistant using CLSI breakpoints.

Additionally, the antibacterial potential of *R. tuberosa* L. extract was assessed via the agar well diffusion assay, following established protocols (29). Standardized suspensions of *E. coli* and *K. pneumoniae*, adjusted to a final density of $1.5x10^8$ CFU/ml (0.5 McFarland standard), were uniformly swabbed onto MHA plates. An 8-mm well was aseptically created in the agar using a sterile cork borer, into which 40 μl of the extract (dissolved in DMSO at 50 mg/ml) was pipetted. Pure DMSO (Rankem Laboratories, LLC) served as the negative control. The plates were incubated at 37˚C for 24 h, following which the diameters of the inhibition zones were accurately measured in mm using a vernier calliper to assess antibacterial activity.

Broth microdilution method. The MIC of *R. tuberosa* L. extract was determined using a 2-fold broth microdilution method, as previously described (30). Briefly, concentrations ranging from 40-0.078 mg/ml were tested by inoculating standardized suspensions of *E. coli* and *K. pneumoniae* ($1.5x10^8$ CFU/ml) into BHI broth containing *R. tuberosa* L. extract. The mixtures were incubated at 37˚C for 24 h. Post-incubation, 2,3,5-triphenyltetrazolium chloride (TTC) (HiMedia Laboratories Private Limited) was added to each well to detect viable cells through color development. The lowest concentration exhibiting no color change was recorded as the MIC. Based on the MIC values obtained, subsequent biofilm inhibition assays were conducted using sub-MIC concentrations derived from these preliminary determinations to specifically assess growth-independent antibiofilm activity.

Biofilm quantification assay. The impact of *R. tuberosa* L. extract on biofilm formation by *E. coli* and *K. pneumoniae* was assessed using a previously described crystal violet (CV) staining method with slight modifications (31). Briefly, microtiter plates containing 180 μl fresh BHI medium were inoculated with 20 μl of overnight culture of the test organisms. Subsequently, *R. tuberosa L.* extract was added at sub-MIC concentrations (*E. coli*: 10 to 0.019 mg/ml; *K. pneumoniae*: 20 to 0.039 mg/ml), and the plates were incubated at 37˚C for 48 h. Adherent biofilms were then stained with 0.1% CV solution (HiMedia Laboratories) for 15 min at room temperature, followed by washing with phosphate-buffered saline (PBS) (HiMedia Laboratories Private Limited) to remove planktonic cells. Bound CV was eluted with 200 μl of 70% ethanol following a 5-min incubation at 37˚C, and the absorbance was measured at 525 nm using a UV-Vis spectrophotometer (JASCO).

Growth kinetics analysis of E. coli and K. pneumoniae. The growth kinetics of *E. coli* and *K. pneumoniae* were evaluated in the presence of *R. tuberosa* L. extract at sub-MIC concentration. For *E. coli*, bacterial growth was assessed at a sub-MIC of 10 mg/ml, whereas for *K. pneumoniae*, growth kinetics were evaluated at a sub-MIC of 20 mg/ml. Overnight cultures were supplemented with the extract and incubated at 37˚C for 24 h. Bacterial cell density was monitored hourly by measuring the optical density (OD_{600}) using a spectrophotometer (JASCO).

GC-MS profiling of R. tuberosa L. extract. For GC-MS analysis, the dried ethanolic extract of *R. tuberosa* L. was reconstituted in n-hexane at a final concentration of 1 mg/ml. The analysis was performed according to a previously described protocol, with minor modifications adapted for the present study (32). An aliquot (1 μl) was injected in split mode (100:1) using an AOC-5000 autosampler (Shimadzu Corporation). Analysis was performed on a Shimadzu GCMS-QP2010 Plus system equipped with an RTx-5MS capillary column (cross-bond diphenyl dimethyl polysiloxane-fused silica) (Shimadzu Corporation). Ultra-high-purity helium (≥99.99%) served as the carrier gas at a constant flow rate of 0.8 ml/min. Compound identification was achieved by comparison of mass spectra with the NIST/WILEY7 library (John Wiley & Sons), and only compounds with a match quality ≥80% were accepted. GC-MS was conducted for qualitative phytochemical profiling only; individual compounds were not isolated for *in-vitro* testing. Biological assays were performed using the crude extract, and GC-MS results were used solely to guide compound selection for *in silico* docking analysis.

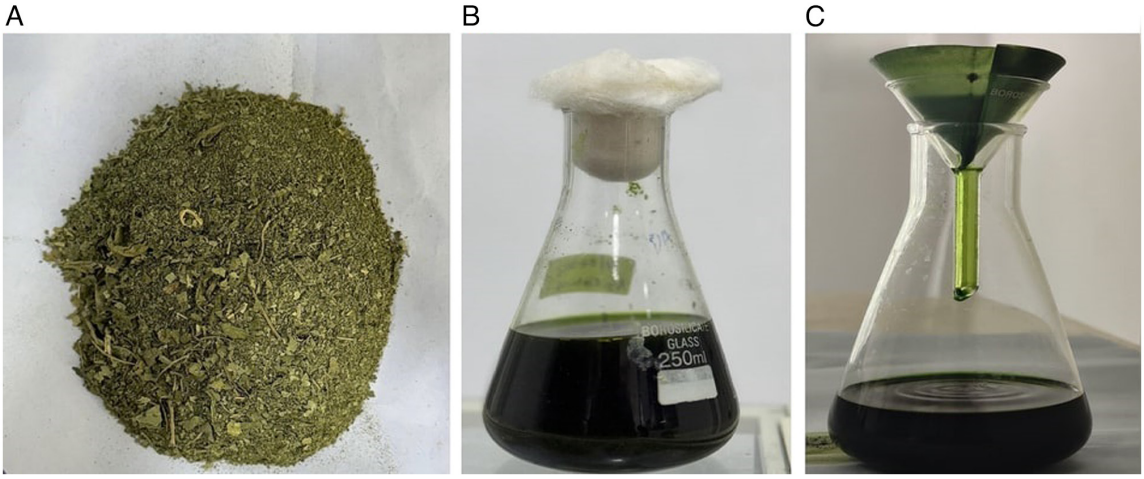

Figure 1. Preparation of *Ruellia tuberosa* L. ethanolic leaf extract. (A) Shade-dried powdered leaves. (B) Maceration in ethanol (4 days). (C) Filtration of the extract.

Computational analysis of compounds from R. tuberosa L. extract. In silico molecular docking analysis was conducted on compounds identified from the *R. tuberosa* L. ethanolic extract. GC-MS profiling revealed multiple phytochemicals, with diethyl phthalate [DEP, 42.56%; relative abundance, retention time (RT) 14.98 min] as the most prominent constituent. DEP was selected for docking analysis based on its relative abundance in the extract, serving as a representative compound for preliminary assessment of potential protein-ligand interactions.

Docking-based interaction analysis. DEP ($C_{12}H_{14}O_4$; PubChem CID: 6781) has a molecular weight of 222.24 g/mol and consists of 12 carbon atoms, 14 hydrogen atoms and 4 oxygen atoms. DEP was detected in the GC-MS chromatogram through its prominent high-intensity peak, exhibiting the highest relative abundance based on peak area. Its chemical structure was retrieved and verified using PubChem database information (NCBI, NIH).

Structure-based molecular docking and binding interaction analysis. For molecular docking analysis, only the biologically relevant monomeric chain (Chain A) of each protein was retained, while all other chains, crystallographic water molecules, and co-crystallized ligands were removed to prevent potential interference during binding simulations. The present study targeted key proteins implicated in biofilm formation and virulence in *E. coli* and *K. pneumoniae*. The selected structures included 8ENQ (cryo-EM structure of *E. coli* CsgA fibril), 5DFK (crystal structure of *E. coli* common pilus chaperone EcpB), 8FFK (apo structure of the *K. pneumoniae* AcrB multidrug efflux pump), and 9HW9 (solution NMR structure of the type 3 fimbrial subunit MrkA from *K. pneumoniae*). Three-dimensional coordinates of these proteins were retrieved from the RCSB Protein Data Bank (PDB). Protein preparation involved the removal of H_2O molecules, non-essential chains, and bound ligands, followed by the addition of polar hydrogens and assignment of appropriate atomic charges using BIOVIA Discovery Studio Visualizer 2024 (v24.1.0.23298, Dassault Systèmes Biovia Corp.).

Computational docking analyses were conducted to evaluate the interaction of DEP with the selected protein targets. Docking simulations were performed using PyRx-Python Prescription 0.8 integrated with AutoDock Vina. The grid box center coordinates and dimensions were defined to encompass the predicted active or binding regions of each protein, and the detailed parameters used for each target are provided in Table SI to ensure computational reproducibility. Multiple ligand conformations were generated, and the most favorable docking pose for each protein-ligand complex was selected based on the lowest (most negative) binding energy values. The final binding modes and three-dimensional interaction patterns were visualized and analyzed using BIOVIA Discovery Studio Visualizer 2024.

Statistical analysis. All assays were performed in triplicate, and data are presented as the mean ± SD. Statistical analysis was performed using one-way ANOVA followed by Tukey's post hoc test in GraphPad Prism (v5.03; Dotmatics) and was used to analyze biofilm and growth curve data. A value of $P<0.05$ was considered to indicate a statistically significant difference compared to the controls.

Results

Identification of E. coli and K. pneumoniae. E. coli and *K. pneumoniae* were accurately confirmed via the automated VITEK® 2 system (https://www.biomerieux.com). Complementary validation was achieved through distinctive colony morphology and growth characteristics on MacConkey agar (Fig. 2).

Antibiogram and antimicrobial analysis. Antibiogram analysis adhered to CLSI guidelines. Both *E. coli* and *K. pneumonia* isolates exhibited substantial resistance to most tested antibiotics including ampicillin, ceftriaxone, ciprofloxacin and gentamicin. Susceptibility persisted primarily to last-line options imipenem and colistin (Table I). The antimicrobial potential of *R. tuberosa* L. extract was evaluated using the agar well diffusion method against *E. coli* and *K. pneumoniae*. The results revealed a distinct zone of inhibition measuring 14 mm and 13 mm, indicating a significant level

Table I. Comparative antibiotic susceptibility profile of clinical *E. coli* and *K. pneumoniae* isolates determined by the Kirby-Bauer disk diffusion method according to CLSI guidelines.

Antibiotic	*E. coli* (mean ± SD, mm)	Interpretation	*K. pneumoniae* (mean ± SD, mm)	Interpretation
Ampicillin	No zone	Resistant	No zone	Resistant
Ceftriaxone	No zone	Resistant	12±1.3	Resistant
Ciprofloxacin	14±1.2	Resistant	14±1.2	Resistant
Gentamicin	14±1.1	Resistant	14±0.5	Resistant
Imipenem	20±1.3	Sensitive	20±1.4	Sensitive
Colistin	21±1.2	Sensitive	22±1.3	Sensitive

Results are expressed as mean zone diameter (mm) ± SD. CLSI, Clinical and Laboratory Standards Institute; *E. coli, Escherichia coli; K. pneumoniae, Klebsiella pneumoniae*.

Table II. Minimum inhibitory concentration of *R. tuberosa* L. against *E. coli and K. pneumoniae*.

		Growth measured	
Serial no.	Two-fold dilution concentration (mg/ml)	*E. coli*	*K. pneumoniae*
Sl.1	40	-	-
2	20	-	+
3	10	+	+
4	5	+	+
5	2.5	+	+
6	1.25	+	+
7	0.625	+	+
8	0.312	+	+
9	0.156	+	+
10	0.078	+	+

R. tuberosa L, *Ruellia tuberosa* L.; *E. coli, Escherichia coli; K. pneumoniae, Klebsiella pneumoniae; -, growth inhibited; +, growth*.

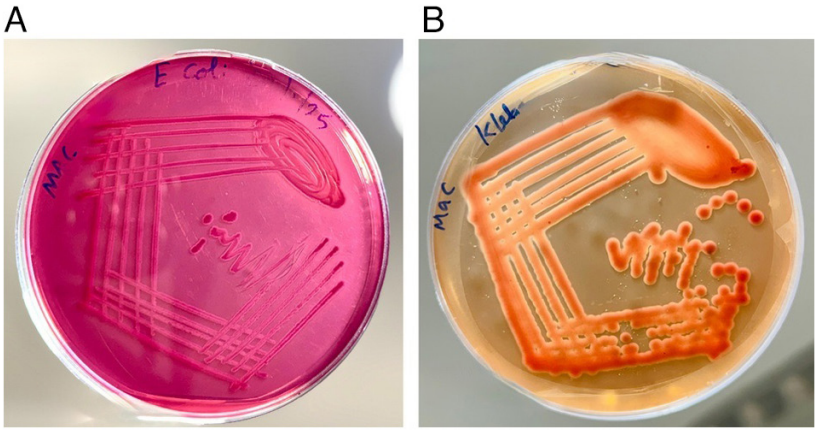

Figure 2. Identification of bacterial isolates on MacConkey agar. (A) *E. coli* exhibiting lactose-fermenting pink colonies. (B) *K.pneumoniae* exhibiting large mucoid lactose-fermenting colonies.

of antimicrobial efficacy against this pathogen (Fig. 3). This suggests that *R. tuberosa* L. extract possesses the capability to inhibit the growth of *E. coli* and *K. pneumoniae*, which is particularly relevant given the MDR nature of the pathogen.

MIC analysis of R. tuberosa L. extract. Using a 2-fold serial broth dilution method, the MIC of *R. tuberosa* L. extract was determined to be 20 mg/ml for *E. coli* and 40 mg/ml for *K. pneumoniae* (Table II). Based on these results, sub-MIC

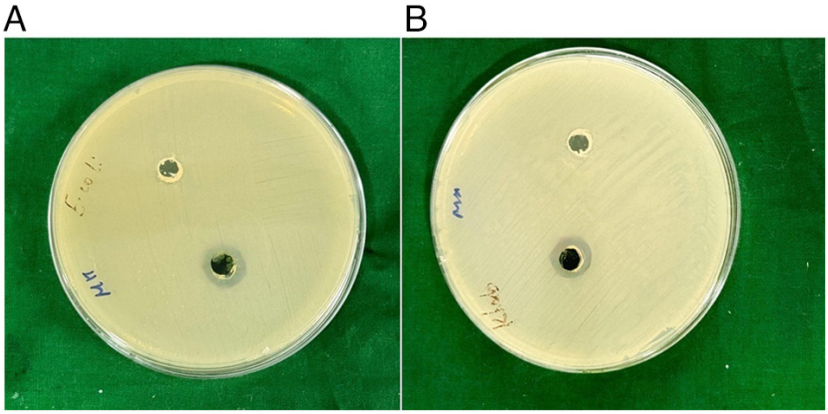

Figure 3. Agar well diffusion assay showing antimicrobial activity of *Ruellia tuberosa* L. extract against (A) *E. coli* and (B) *K. pneumoniae*, with inhibition zones of 14 and 13 mm, respectively, along with the negative control.

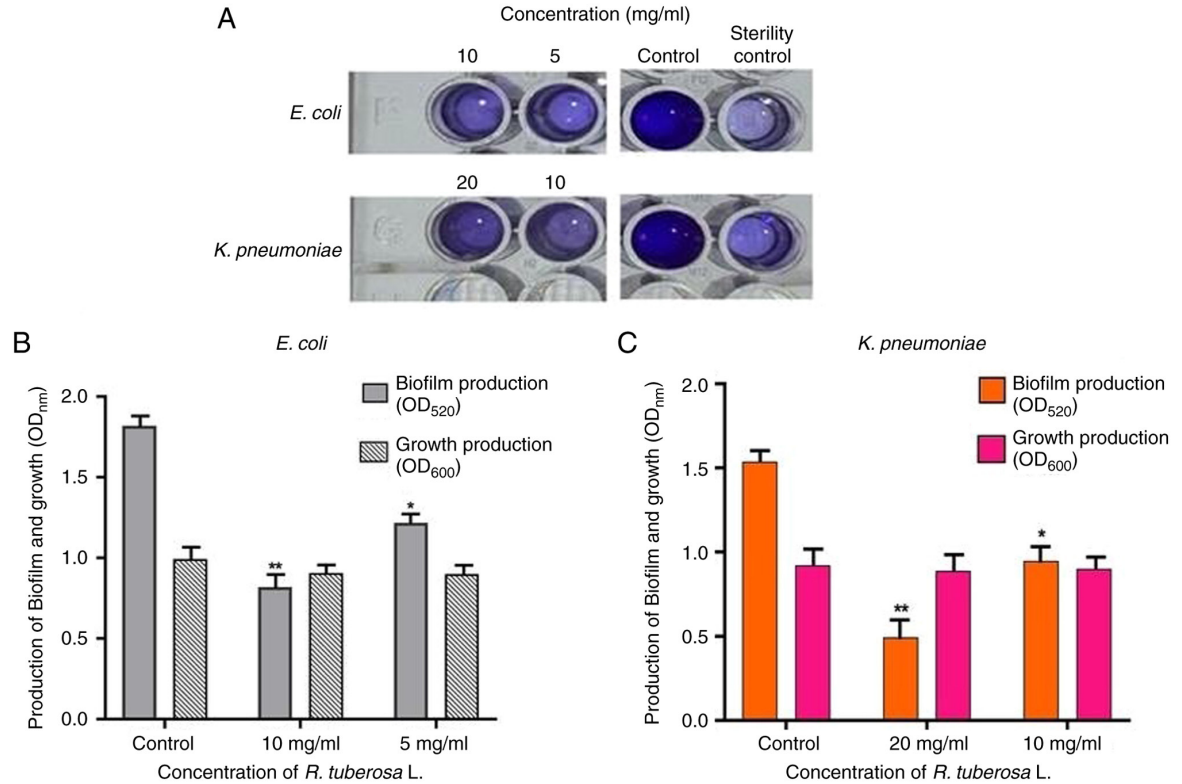

Figure 4. Inhibition of biofilm formation by *R. tuberosa* L. extract. (A) Representative images of CV-stained biofilms of *E. coli* and *K. pneumoniae* at different concentrations, including control and sterility control Biofilm inhibition in (B) *E. coli* and (C) *K. pneumoniae* was quantified using the CV staining assay (OD_{520}), with bacterial growth measured at OD_{600}. The *R. tuberosa* L. extract significantly reduced biofilm formation by 55% in *E. coli* at 10 mg/ml and by 67.81% in *K. pneumoniae* at 20 mg/ml compared to the control. Data are presented as the mean ± SD. $^{*}P<0.05$ and $^{**}P<0.01$. *R. tuberosa* L, *Ruellia tuberosa* L.; *E. coli, Escherichia coli; K. pneumoniae, Klebsiella pneumoniae*.

concentrations were subsequently selected and employed for anti-biofilm assays.

Inhibition of biofilm formation by E. coli and K. pneumoniae. The CV staining biofilm assay demonstrated significant inhibition by *R. tuberosa* L. extract (Fig. 4A). Spectrophotometric analysis at 520 nm (OD_{520}) revealed 55 and 33% biofilm reduction in *E. coli* at 10 and 5 mg/ml, respectively (Fig. 4B). For *K. pneumoniae*, biofilm formation decreased by 67.81% at 20 mg/ml and 38.83% at 10 mg/ml (Fig. 4C). All observed reductions were statistically significant compared to the control ($P<0.05$). The statistical analysis of OD_{600} growth measurements revealed no significant difference between the treated and untreated groups at the tested sub-MIC concentrations, confirming that the observed reductions in biofilm biomass were independent of bacterial growth inhibition.

Growth kinetics analysis. The growth kinetics of *E. coli* and *K. pneumoniae* exhibited comparable patterns upon exposure to the *R. tuberosa* L. extract at sub-MIC levels. *E. coli* was evaluated at a sub-MIC concentration of 10 mg/ml (Fig. 5A), whereas *K. pneumoniae* was assessed at 20 mg/ml. Regardless

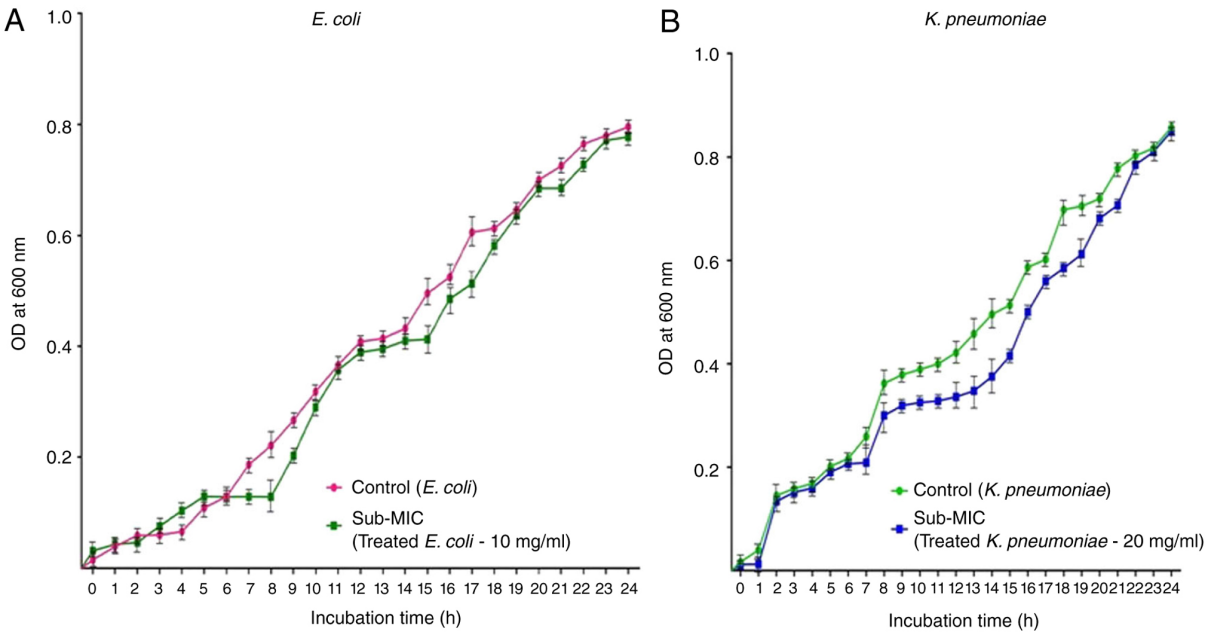

Figure 5. Growth kinetics of *E. coli* and *K. pneumoniae* in the presence of *R. tuberosa* L. extract. Growth curves of (A) *E. coli* and (B) *K. pneumoniae* were monitored at sub-MIC concentrations of *R. tuberosa* L. extract (10 and 20 mg/ml, respectively). Data are presented as the mean ± SD. *R. tuberosa* L, *Ruellia tuberosa* L.; *E. coli*, *Escherichia coli; K. pneumoniae*, *Klebsiella pneumoniae*.

of the observed differences in concentrations, no marked difference in growth was observed between the two species relative to the control (Fig. 5B).

GC-MS analysis of R. tuberosa L. GC-MS profiling of the ethanolic extract of *R. tuberosa* L. identified >30 distinct chemical constituents through matching with the NIST and Wiley spectral libraries (Table III). The chromatograms displayed multiple compounds with distinct RT, featuring diethyl phthalate (DEP; 42.56%; RT, 14.98 min) as the predominant components (Fig. 6). This rich phytochemical diversity underscores the therapeutic promise of *R. tuberosa* L., with DEP selected for further molecular docking analysis due to its highest abundance. The minor baseline drift observed is due to solvent background and column characteristics and did not affect compound identification, as no well-defined peaks in this region satisfied the library match quality criteria.

In silico analysis of DEP interactions with E. coli and K. pneumoniae regulators. DEP was selected for molecular docking based on its highest relative abundance in the GC-MS profile, allowing assessment of one of the major constituents of the extract. Although other compounds such as erucic acid, phytol and octacosanol were also identified and may possess biological activity, the present analysis focused on DEP as a representative constituent for preliminary mechanistic evaluation. Docking simulations were performed to evaluate the binding interactions of DEP with key regulatory and virulence-associated proteins of *E. coli* and *K. pneumoniae*. The selected targets included 8ENQ (cryo-EM structure of *E. coli* CsgA fibril), 5DFK (crystal structure of *E. coli* common pilus chaperone EcpB), 8FFK (apo form of the *K. pneumoniae* AcrB multidrug efflux pump), and 9HW9 (solution NMR structure of the type 3 fimbrial subunit MrkA from *K. pneumoniae*). DEP exhibited binding affinities of -4.00 kcal/mol and -5.2 kcal/mol toward the *E. coli* targets 8ENQ and 5DFK (Table IV), respectively. In *K. pneumoniae*, DEP showed binding energies of -5.4 kcal/mol for 8FFK and -4.6 kcal/mol for 9HW9 (Table V).

Interaction analysis revealed that DEP binding to 8ENQ involved π-π stacking with TRP A:106, along with alkyl and π-alkyl interactions with LEU A:59 and TRP A:106. For the 5DFK protein, DEP formed π-alkyl interactions with PRO A:41, ILE A:120 and TYR A:169 (Fig. 7). In the case of 8FFK, DEP exhibited π-π stacking with PHE A:616 and additional alkyl and π-alkyl interactions with LEU A:572, PHE A:665, ILE A:625, and MET A:574. Notably, DEP formed three conventional hydrogen bonds with 9HW9 involving GLN A:107 (3.01 Å), SER A:154 (2.39 Å) and GLN A:104 (2.62 Å), with bond lengths falling within the typical hydrogen bond distance range. Additionally, a carbon-hydrogen bond was observed with ASN A:105, along with π-alkyl and alkyl interactions involving LEU A:84 and TYR A:94 (Fig. 8). Although the binding energies obtained for DEP (-4.0 to -5.4 kcal/mol) are modest compared to high-affinity drug-target interactions, they fall within the range commonly reported for small, non-drug-like natural compounds involved in anti-virulence and antibiofilm modulation. Similar docking scores have been reported for phytochemicals that exert biologically meaningful effects through multi-target, low-affinity interactions rather than single high-affinity inhibition (22,30).

Discussion

The ability of *E. coli* and *K. pneumoniae* to form robust biofilms is a major contributor to their persistence, virulence and MDR in clinical settings. Biofilm-associated infections are notoriously difficult to eradicate, as embedded cells exhibit enhanced

Table III. GC-MS identification of compounds in *Ruellia tuberosa L.* with corresponding retention times and area percentage.

Serial no. and peak	Name of the compounds	Molecular formula	Retention time	Percentage
1	Benzyl chloride	C_7H_7Cl	6.9116	0.56
2	2,5-Hexanedione	$C_6H_{10}O_2$	7.0354	1.08
3	Dodecane	$C_{12}H_{26}$	9.6500	0.33
4	5-Hydroxymethylfurfural	$C_6H_6O_3$	10.0615	1.00
5	Tetradecane	$C_{14}H_{30}$	12.4430	0.32
6	1,1,6-Trimethyl-1,2-dihydronaphthalene	$C_{13}H_{16}$	12.6142	0.24
7	5-Methylene-4,5,6,6a-tetrahydro-3ah-pentalen-1-one	$C_9H_{10}O$	13.3170	0.25
8	Phorone	$C_9H_{14}O$	13.5901	0.33
9	1,4-Dihydrothujopsene-(I1)	$C_{15}H_{26}$	13.8705	0.25
10	Diethyl phthalate	$C_{12}H_{14}O_4$	14.9811	42.56
11	Terpinyl propionate	$C_{13}H_{22}O_2$	16.2193	0.32
12	Tetradecanoic acid	$C_{14}H_{28}O_2$	16.7546	0.51
13	Loliolide	$C_{11}H_{16}O_3$	17.0204	0.54
14	Beta-homocyclocitral	$C_{11}H_{18}O$	17.3955	0.52
15	Isopropyl myristate	$C_{17}H_{34}O_2$	17.4464	0.56
16	Erucic acid	$C_{22}H_{42}O_2$	17.5994	6.29
17	3,7,11,15-Tetramethyl-2-hexadecen-1-ol	$C_{20}H_{40}O$	17.6686	0.84
18	Linolenic acid	$C_{18}H_{30}O_2$	17.8560	5.22
19	Isooctanol	$C_8H_{18}0$	17.8980	0.92
20	2-Hexadecen-1-ol, 3,7,11,15-tetramethyl-, acetate, [R [R*,R*-(E)]]	C22H42O2	18.0510	7.77
21	Cholest-5-ene, 3 bromo-, (3á)-	C27H45Br	18.2730	2.98
22	n-Hexadecanoic acid	$C_{16}H_{32}O_2$	18.8521	1.79
23	Hexadecanoic acid, ethyl ester	$C_{18}H_{36}O_2$	19.1725	0.65
24	2H-Pyran-2-one	$C_5H_4O_2$	20.0610	0.43
25	Phytol	$C_{20}H_{40}O$	20.3123	3.16
26	13Z,16Z-docosadienoic acid	$C_{22}H_{40}O_2$	20.5672	5.96
27	Octacosanol	$C_{28}H_{58}O$	20.6437	3.59
28	Linoleic acid ethyl ester	$C_{20}H_{36}O_2$	20.7602	0.34
29	Dihomo-gamma-linolenic acid	$C_{20}H_{34}O_2$	20.8185	0.64
30	1-O-hexadecyl-2-(9Z-octadecenoyl)-sn-glycerol	$C_{37}H_{72}O_4$	23.2874	0.23
31	Glycerol 1-palmitate	$C_{19}H_{38}O_4$	23.5569	0.31
32	Bis(2-ethylhexyl) phthalate	$C_{24}H_{38}O_4$	23.9064	0.53
33	Octacosanol	$C_{28}H_{58}O$	25.6471	8.04
34	Squalene	$C_{30}H_{50}$	26.0076	0.94

Peak numbers align with those illustrated in Fig. 6. GC-MS, gas chromatography-mass spectrometry.

tolerance to antibiotics and host immune responses (33). Therefore, identifying natural agents that disrupt biofilm formation without exerting strong bactericidal pressure is a critical strategy to mitigate resistance development.

In the present study, preliminary antibiogram analysis revealed that the clinical isolate of *E. coli* and *K. pneumoniae* exhibited resistance to the majority of the tested antibiotics. Owing to this MDR profile, the present study subsequently evaluated the antimicrobial potential of the ethanolic leaf extract of *R. tuberosa* L. The extract demonstrated appreciable antibacterial activity against *E. coli* and *K. pneumoniae*, producing zones of inhibition of 14 and 13 mm, respectively, at a concentration of 50 mg/ml in the agar well diffusion assay. These findings align closely with values documented in prior studies for *R. tuberosa* ethanolic or n-hexane extracts, which typically produced inhibition zones of 7-16 mm only at the highest tested concentrations (26); notably, in the present study, similar inhibitory effects were achieved at substantially lower concentrations against *E. coli* and *K. pneumoniae*. Similarly, *Tinospora cordifolia* has been reported as an effective source for the biogenic synthesis of ZnO nanoparticles exhibiting notable antimicrobial activity (34). These findings are consistent with the results of the present study and

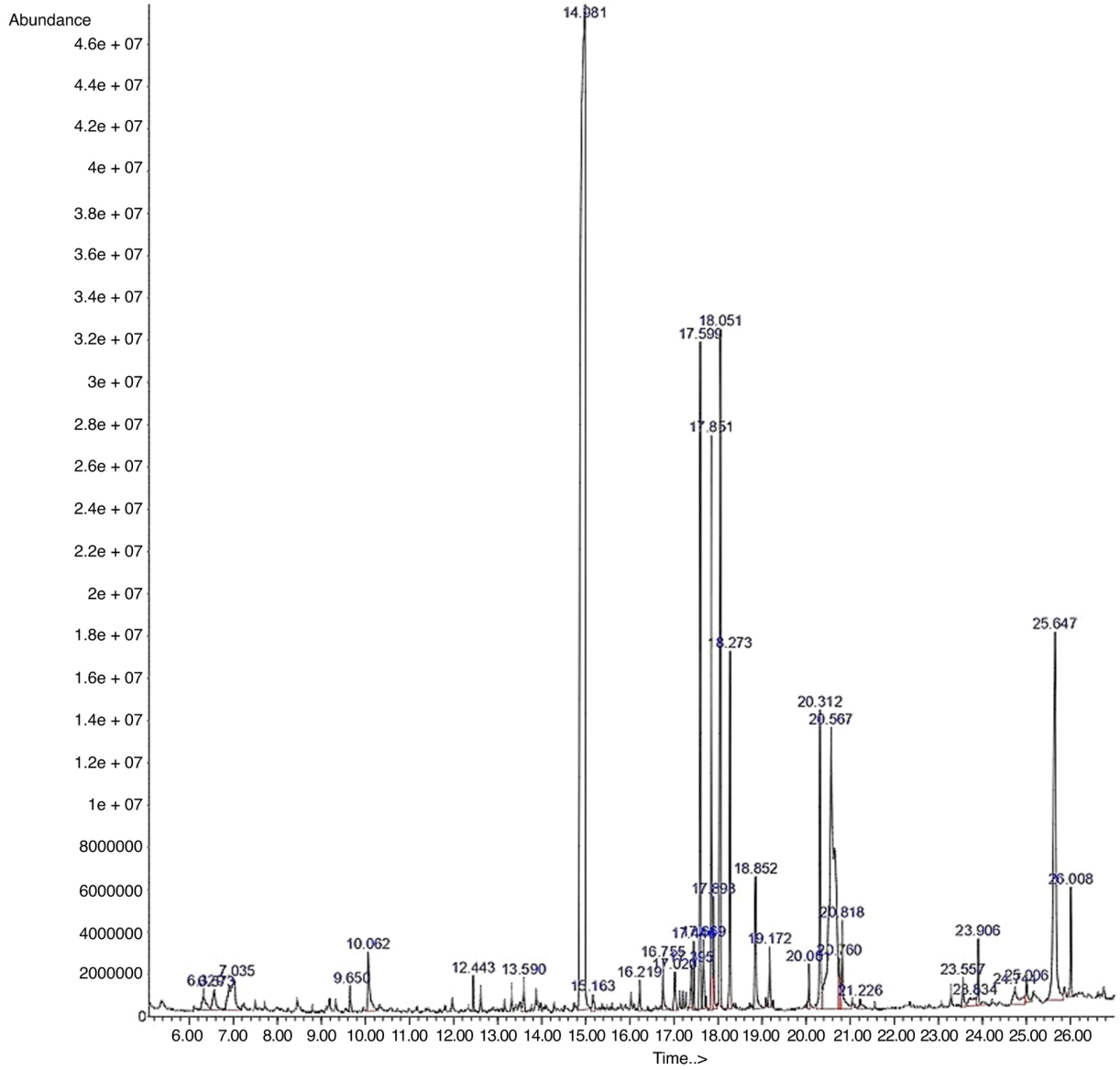

Figure 6. Gas chromatography-mass spectrometry chromatogram of *Ruellia tuberosa* L. Spectral peaks were analyzed using the WILEY7 library, and the identified compounds are summarized in Table III. Peak 10, detected at a retention time of 14.98 min, exhibited the highest relative abundance.

further support the potential of plant-derived systems for antimicrobial applications at low concentrations.

MIC analysis further highlighted the potency of the extract, with MIC values of 20 mg/ml for *E. coli* and 40 mg/ml for *K. pneumoniae*. These concentrations are markedly lower than those reported in earlier studies, such as in the study by Amajida *et al* (26), who observed inhibition of *E. coli* and *Bacillus subtilis* only at 500 mg/ml. The lower MIC values observed in the present study may reflect differences in phytochemical composition, extraction efficiency and strain-specific susceptibility. In addition, methodological variations including solvent type, extraction duration, plant source variability, and growth conditions employed during antimicrobial assays may also contribute to the discrepancies observed when compared with previous reports, including the study by Amajida *et al* (26).

Moreover, a key strength of the present study lies in the sub-MIC antibiofilm evaluation, which revealed substantial inhibition of biofilm formation without affecting planktonic growth. At the sub-MIC level, the extract inhibited biofilm formation by 55% in *E. coli* (10 mg/ml) and 67.81% in *K. pneumoniae* (20 mg/ml), while growth kinetics (OD_{600}) remained indistinguishable from the untreated controls. This growth neutrality strongly indicates a true antibiofilm mechanism. Similar antibiofilm effects have been reported in previous research for several natural phenolic compounds, including epigallocatechin gallate, octyl gallate, scutellarein, wedelolactone and resveratrol, which reduce *E. coli* biofilm formation by 50-80% at sub-MIC concentrations through the suppression of curli expression, motility and chemotactic responses (35). Additionally, a number of essential oils and plant-derived agents (e.g., cinnamaldehyde and eugenol) also impair membrane integrity or significantly alter growth and motility, making it difficult to distinguish antibiofilm-specific effects from general antibacterial stress (36-37). By contrast, *R. tuberosa* extract achieved comparable biofilm inhibition, while fully sparing

Table IV. Molecular docking results of DEP with *E. coli* targets 8ENQ and 5DFK.

Binding of DEP with *E. coli* targets 8ENQ and 5DFK	Binding affinity	rmsd/ub	rmsd/lb
8ENQ_6781_ E=211.67	-4	0	0
8ENQ_6781_E=211.67	-3.9	31.488	28.751
8ENQ_6781_E=211.67	-3.9	34.752	32.937
8ENQ_6781_ E=211.67	-3.9	31.964	30.064
8ENQ_6781_ E=211.67	-3.8	32.266	29.807
8ENQ_6781_ E=211.67	-3.8	31.754	29.339
8ENQ_6781_ E=211.67	-3.8	30.881	29.36
8ENQ_6781_ E=211.67	-3.7	34.065	32.006
8ENQ_6781_ E=211.67	-3.7	34.363	31.683
5DFK_6781_E=211.67	-5.2	0	0
5DFK_6781_ E=211.67	-5.2	3.542	1.13
5DFK_6781_E=211.67	-5.1	11.338	9.815
5DFK_6781_E=211.67	-5.1	3.63	1.379
5DFK_6781_E=211.67	-5.1	11.271	9.789
5DFK_6781_ E=211.67	-4.9	2.342	1.534
5DFK_6781_ E=211.67	-4.8	14.807	12.768
5DFK_6781_ E=211.67	-4.7	12.057	10.719
5DFK_6781 _E=211.67	-4.6	11.588	10.441

The table presents a summary of the binding affinities (kcal/mol) and corresponding docking poses of DEP against the 8ENQ and 5DFK proteins. The column headers 'rmsd/ub' and 'rmsd/lb' refer to the root-mean-square deviation upper bound and lower bound, respectively, which indicate the positional deviation between docking poses. DEP exhibited binding energies of -4.00 kcal/mol for 8ENQ and -5.2 kcal/mol for 5DFK. DEP, diethyl phthalate; *E. coli*, *Escherichia coli*.

Table V. Molecular docking analysis of DEP with *K. pneumoniae* targets 8FFK and 9HW9.

Binding of DEP with *K. pneumoniae* targets 8FFK and 9HW9	Binding affinity	rmsd/ub	rmsd/lb
8FFK_6781_E=211.67	-5.4	0	0
8FFK_6781_E=211.67	-5.4	4.241	0.071
8FFK_6781_E=211.67	-5.4	19.269	17.333
8FFK_6781_E=211.67	-5.3	19.879	17.537
8FFK_6781_E=211.67	-5.3	3.664	1.197
8FFK_6781_E=211.67	-5.3	2.101	1.282
8FFK_6781_E=211.67	-5.2	19.48	17.171
8FFK_6781_E=211.67	-5.2	20.076	17.843
8FFK_6781_E=211.67	-5.1	30.794	28.043
9HW9_ 6781_E=211.67	-4.6	0	0
9HW9_ 6781_E=211.67	-4.5	4.513	2.415
9HW9_ 6781_E=211.67	-4.4	21.575	19.773
9HW9_ 6781_E=211.67	-4.3	8.499	6.76
9HW9_ 6781_E=211.67	-4.3	20.282	18.199
9HW9_ 6781_E=211.67	-4.3	20.033	18.223
9HW9_ 6781_E=211.67	-4.3	21.633	19.821
9HW9_ 6781_E=211.67	-4.3	21.658	19.916
9HW9_ 6781_E=211.67	-4.1	15.602	13.318

Summarizes the binding affinities (kcal/mol) and corresponding docking poses of DEP against the 8FFK and 9HW9 proteins. The column headers 'rmsd/ub' and 'rmsd/lb' denote the root-mean-square deviation upper bound and lower bound, respectively, indicating the positional deviation between predicted docking conformations. DEP exhibited binding energies of -5.4 kcal/mol for 8FFK and -4.6 kcal/mol for 9HW9. DEP, diethyl phthalate; *K. pneumoniae*, *Klebsiella pneumoniae*.

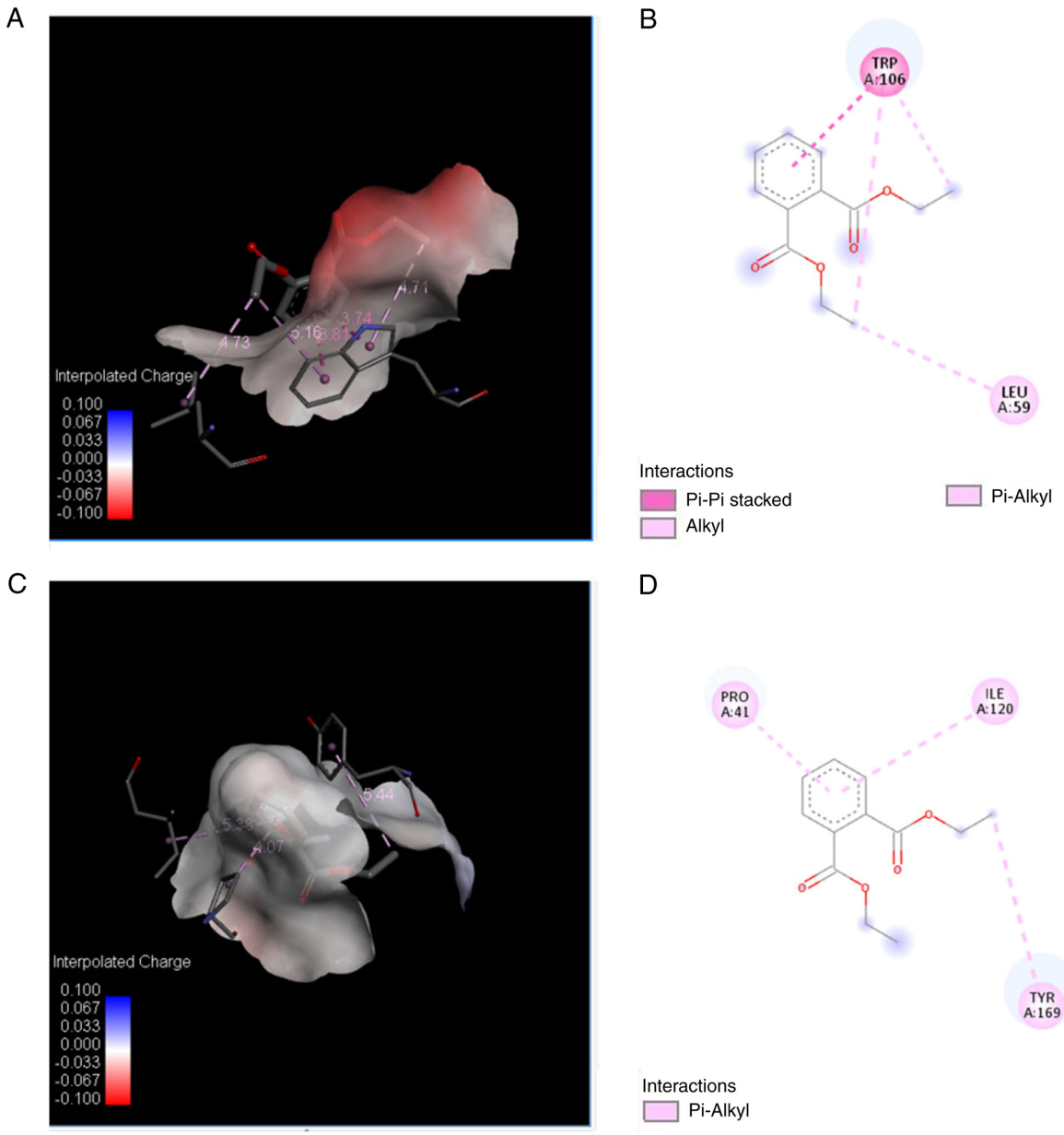

Figure 7. Molecular interaction analysis of DEP with *E. coli* target proteins. (A and C) 3D binding poses of DEP within the active sites of 8ENQ and 5DFK proteins, respectively, shown as electrostatic surface representations; (B and D) 2D interaction maps illustrating key stabilizing interactions. In the 2D diagrams, dark pink dashed lines indicate π-π stacking interactions, light pink dashed lines represent π-alkyl interactions, and pink lines denote alkyl interactions. DEP binding to 8ENQ is characterized by π-π stacking with TRP A:106 and alkyl/π-alkyl interactions with LEU A:59 and TRP A:106. Interactions with 5DFK involve π-alkyl contacts with PRO A:41, ILE A:120, and TYR A:169.

planktonic growth, suggesting that it may represent a promising anti-virulence candidate capable of inhibiting biofilm formation without affecting planktonic growth. Similar antibiofilm activities have been observed with other plant extracts in different Gram-negative species, such as *Rhamnus frangula* against *Acinetobacter baumannii* at 5 mg/ml (38). Additionally, *R. officinalis* and *P. paniculata* are known to impede biofilm formation in *K. pneumoniae* by up to 58.41 and 55.71%, respectively (39). In comparison with these reports, in the present study, *R. tuberosa* extract exhibited comparable antibiofilm activity against *E. coli* and *K. pneumoniae*, highlighting its potential as an effective antibiofilm agent.

Several natural products, including *Coffea arabica* L. extracts, promysalin, and specialized microbial metabolites, are known to inhibit biofilm formation at sub-MIC or nanomolar concentrations through defined molecular targets (40-42). While these compounds are highly potent, they are often structurally complex (e.g., promysalin requiring multi-step total synthesis), difficult to source (microbial fermentation-dependent), or associated with specific metabolic targets (e.g., succinate dehydrogenase) that may limit broader applicability. In contrast, the activity of *R. tuberosa* L. extract appears to arise from a multi-target, phytochemical-driven mechanism, which may reduce the likelihood of resistance development, while enhancing compatibility with existing antibiotics.

In the present study, the GC-MS profiling of the *R. tuberosa* extract identified >30 compounds, with DEP (42.56% relative abundance) as the predominant constituent. To explore potential

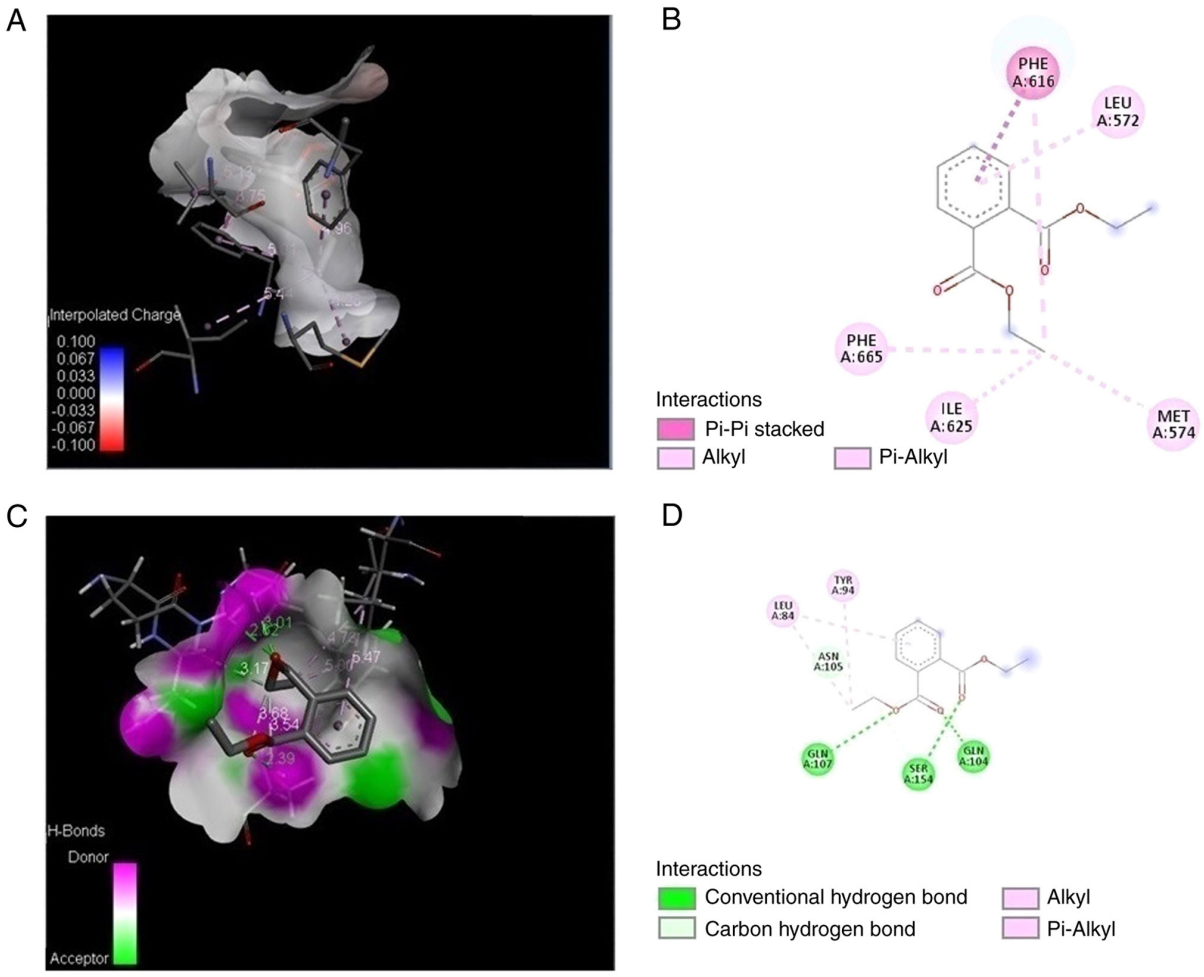

Figure 8. Molecular docking and interaction analysis of *K. pneumoniae* proteins. (A and C) 3D binding conformations of DEP within the active sites of 8FFK and 9HW9, shown as surface representations; (B and D) 2D interaction diagrams highlighting key stabilizing interactions. In the 2D maps, green dashed lines represent conventional hydrogen bonds, light green dashed lines indicate carbon-hydrogen bonds, pink lines denote alkyl interactions, light pink dashed lines indicate π-alkyl interactions, and dark pink dashed lines represent π-π stacking interactions. DEP binding to 8FFK is characterized by π-π stacking with PHE A:616 and alkyl/π-alkyl interactions involving LEU A:572, PHE A:665, ILE A:625, and MET A:574. By contrast, DEP interaction with 9HW9 involves three conventional hydrogen bonds with GLN A:107, SER A:154, and GLN A:104, a carbon-hydrogen bond with ASN A:105, and additional alkyl/π-alkyl interactions with LEU A:84 and TYR A:94.

molecular interactions underlying the observed antibiofilm activity, *in silico* docking analyses were performed. For clarity, only the principal binding interactions and key stabilizing residues are summarized. DEP exhibited stable interactions with major biofilm and resistance-associated targets, including the *E. coli* CsgA curli fibril (-4.0 kcal/mol, π-stacking with TRP A:106), EcpB chaperone (-5.2 kcal/mol), *K. pneumoniae* AcrB efflux pump (-5.4 kcal/mol, π-stacking with PHE A:616) and MrkA fimbrial protein (-4.6 kcal/mol, hydrogen bonding with GLN and SER residues). These findings suggest that DEP may contribute to the observed bioactivity; however, the potential role of other phytoconstituents and synergistic interactions cannot be excluded. DEP may affect bacterial virulence and biofilm formation through multiple mechanisms, including disruption of cell membrane integrity, interference with QS, inhibition of adhesion and fimbriae-associated proteins, and modulation of efflux-related pathways. Previous studies indicate that DEP can exert antibiofilm and anti-virulence effects (43,44). Additionally, DEP has been reported to alter membrane permeability and lipid organization, leading to impaired surface attachment and early biofilm establishment (45,46). In the present study, the observed docking interactions with adhesion and fimbrial-related proteins further support a possible role for DEP in disrupting bacterial attachment and biofilm maturation. Moreover, interactions with efflux-associated proteins may also contribute to reduced persistence within the biofilm matrix. While these mechanisms are supported by *in silico* predictions and previous reports, experimental validation will be required to confirm the relative contribution of each pathway. Further validation using advanced experimental approaches, including *in vitro* and *in vivo* assays, is required to substantiate the antibiofilm potential of DEP. It is important to emphasize that molecular docking provides predictive insights into potential binding interactions and does not constitute functional evidence of target inhibition; therefore, the proposed mechanisms remain hypothetical until validated through targeted biochemical, genetic, or phenotypic assays.

Taken together, the present study advances beyond descriptive antibiofilm observations by integrating quantitative biofilm assays, growth-neutral validation, GC-MS chemical profiling,

and predictive molecular docking to propose a mechanistic framework for anti-virulence activity against clinical MDR pathogens. The findings indicate that *R. tuberosa* L. extract, particularly its major constituent DEP, represents a promising antibiofilm strategy that may enhance antibiotic efficacy and reduce resistance selection when used in combination therapies, particularly for biofilm-associated infections, such as CAUTIs and VAP. However, *in vitro* bioactivity likely reflects the synergistic effects of multiple constituents within the crude extract rather than the action of individual compounds. Accordingly, molecular docking served as a predictive tool to prioritize candidate bioactives, and further validation using purified fractions will be necessary to confirm compound-specific activity.

Nevertheless, the present study has certain limitations. The antibiofilm activity was evaluated using a single clinical isolate each of *E. coli* and *K. pneumoniae*, which limits the generalizability of the findings. These strains were clinical isolates obtained from Saveetha Dental College and Hospitals and identified using the VITEK® 2 system; however, no reference strains were included for comparative analysis. In addition, detailed genotypic characterization, including sequence typing and resistance gene profiling, was not performed. Future studies incorporating a larger and genetically diverse panel of clinical and reference isolates will be necessary to validate and extend the applicability of these findings. Additionally, GC-MS identified the major phytochemical constituents, the individual compounds were not fractionated or tested separately; therefore, the specific bioactive component(s) could not be conclusively determined. Furthermore, *in vivo* validation using appropriate infection models will be essential to establish the therapeutic potential, safety profile, and translational relevance of *R. tuberosa* L. for possible clinical application.

In conclusion, the present study demonstrates that the ethanolic leaf extract of *R. tuberosa* L. exerts significant, growth-neutral antibiofilm effects against MDR *E. coli* and *K. pneumoniae*, with sub-MIC concentrations reducing biofilm biomass, while leaving planktonic growth largely unaffected, consistent with an anti-virulence rather than bactericidal mode of action. GC-MS profiling coupled with molecular docking identified DEP as a major constituent and predicted its potential interactions with key biofilm- and virulence-associated proteins, including curli fibrils and pilus assembly factors in *E. coli* and efflux pump and fimbrial components in *K. pneumoniae*, providing a plausible mechanistic hypothesis rather than direct functional evidence for the observed inhibition of adhesion and biofilm maturation. Altogether, these findings suggest that *R. tuberosa* L. represents a promising phytochemical resource for the development of anti-virulence adjuncts to conventional antibiotics in the management of biofilm-associated infections caused by MDR Gram-negative pathogens, warranting further validation through expanded strain panels, detailed omics-based pathway analysis, and *in vivo* infection models.

Acknowledgements

Not applicable.

Funding

No funding was received.

Availability of data and materials

The data generated in the present study may be requested from the corresponding author.

Authors' contributions

AC contributed to the study design, data collection and manuscript preparation. AB was involved in data collection, data analysis and in the drafting of the manuscript. GRV supervised the study, contributed to data interpretation, and critically revised the manuscript. All authors confirm the authenticity of all the raw data. All authors have read, and approved the final version of the manuscript.

Ethics approval and consent to participate

The bacterial isolates used in the present study were provided as a laboratory gift from the Department of Microbiology, Saveetha Dental College and Hospitals, Chennai, India, at an earlier time and were subsequently transferred to Kannur University, Kerala, for research purposes. The isolates were obtained from the hospital and were transferred by the laboratory authorities to the Kannur University laboratory for research use. The present study did not involve direct patient interaction, access to patient records, or collection of clinical specimens. The isolates were handled strictly as microbiological strains for *in vitro* experimental purposes. Upon receipt, the isolates were reconfirmed in the laboratory based on standard morphological characteristics prior to experimental use. As the study involved only de-identified bacterial isolates and did not include human participants or identifiable patient data, ethics approval and informed patient consent were waived.

Patient consent for publication

Not applicable.

Competing interests

The authors declare that they have no competing interests.

References

1. Liu HY, Prentice EL and Webber MA: Mechanisms of antimicrobial resistance in biofilms. NPJ Antimicrob Resist 2: 27, 2024.
2. Luo Y, Yang Q, Zhang D and Yan W: Mechanisms and control strategies of antibiotic resistance in pathological biofilms. J Microbiol Biotechnol 31: 1-7, 2021.
3. Maldonado RF, Sá-Correia I and Valvano MA: Lipopolysaccharide modification in Gram-negative bacteria during chronic infection. FEMS Microbiol Rev 40: 480-493, 2016.
4. Vuotto C, Longo F, Balice M, Donelli G and Varaldo P: Antibiotic resistance related to biofilm formation in *Klebsiella pneumoniae*. Pathogens 3: 743-758, 2014.
5. Stahlhut SG, Struve C, Krogfelt KA and Reisner A: Biofilm formation of *Klebsiella pneumoniae* on urethral catheters requires either type 1 or type 3 fimbriae. FEMS Immunol Med Microbiol 65: 350-359, 2012.
6. Surgers L, Boyd A, Girard PM, Arlet G and Decré D: Biofilm formation by ESBL-producing strains of *Escherichia coli* and *Klebsiella pneumoniae*. Int J Med Microbiol 309: 13-18, 2019.
7. Lüthje P and Brauner A: Virulence factors of Uropathogenic *E. coli* and their interaction with the Host. Adv Microb Physiol 65: 337-372, 2014.

8. Subashchandrabose S and Mobley HLT: Virulence and fitness determinants of uropathogenic *Escherichia coli*. Microbiol Spectr 3: 10.1128/microbiolspec.UTI-0015-2012, 2015.
9. de Pace F, Nakazato G, Pacheco A, Boldrin de Paiva J, Sperandio V and Dias da Silveira W: The type VI Secretion system plays a role in type 1 fimbria expression and pathogenesis of an avian pathogenic *Escherichia coli* strain. Infect Immun 78: 4990-4998, 2010.
10. Rendón MA, Saldaña Z, Erdem AL, Monteiro-Neto V, Vázquez A, Kaper JB, Puente JL and Girón JA: Commensal and pathogenic *Escherichia coli* use a common pilus adherence factor for epithelial cell colonization. Proc Natl Acad Sci USA 104: 10637-10642, 2007.
11. Xu L, Li J, Wu W, Wu X and Ren J: *Klebsiella pneumoniae* capsular polysaccharide: Mechanism in regulation of synthesis, virulence, and pathogenicity. Virulence 15: 2439509, 2024.
12. Langstraat J, Bohse M and Clegg S: Type 3 fimbrial shaft (MrkA) of *Klebsiella pneumoniae*, but not the *Fimbrial adhesin* (MrkD), facilitates biofilm formation. Infect Immun 69: 5805-5812, 2001.
13. Li Y and Ni M: Regulation of biofilm formation in *Klebsiella pneumoniae*. Front Microbiol 14: 1238482, 2023.
14. Yan J, Pu S, Jia X, Xu X, Yang S, Shi J, Sun S and Zhang L: Multidrug resistance mechanisms of carbapenem resistant *Klebsiella pneumoniae* strains isolated in Chongqing, China. Ann Lab Med 37: 398-407, 2017.
15. Liu X, Sai F, Li L, Zhu C and Huang H: Clinical characteristics and risk factors of catheter-associated urinary tract infections caused by *Klebsiella pneumoniae*. Ann Palliat Med 9: 2668-2677, 2020.
16. Kushnareva M, Markhulia Kh M, Keshishyan E and Semenov A: Ventilator-associated pneumonia caused by *Klebsiella pneumoniae* in preterm newborn infants. Int J Pediatric Res 4: 2469-5769, 2018.
17. Woo S, Marquez L, Crandall WJ, Risener CJ and Quave CL: Recent advances in the discovery of plant-derived antimicrobial natural products to combat antimicrobial resistant pathogens: Insights from 2018-2022. Nat Prod Rep 40: 1271-1290, 2023.
18. Lu L, Hu W, Tian Z, Yuan D, Yi G, Zhou Y, Cheng Q, Zhu J and Li M: Developing natural products as potential anti-biofilm agents. Chin Med 14: 11, 2019.
19. Shamim A, Ali A, Iqbal Z, Mirza MA, Aqil M, Kawish SM, Siddiqui A, Kumar V, Naseef PP, Alshadidi AAF and Saheer Kuruniyan M: Natural medicine a promising candidate in combating microbial biofilm. Antibiotics (Basel) 12: 299, 2023.
20. Bouyahya A, Dakka N, Et-Touys A, Abrini J and Bakri Y: Medicinal plant products targeting quorum sensing for combating bacterial infections. Asian Pac J Trop Med 10: 729-743, 2017.
21. Asfour HZ: Anti-quorum sensing natural compounds. J Microsc Ultrastruct 6: 1-10, 2018.
22. Pathoor NN, Ganesh PS, Gopal RK, Anshad AR, Shankar EM, Mariappan V, Busi S, Salim SA, Kathiresan N, Kulanthaivel L, *et al*: Attenuation of biofilm-encoding genes and virulence attributes in clinical isolates of *Acinetobacter baumannii* by essential oil derived from *Myroxylon balsamum*. Sci Rep 16: 2861, 2026.
23. Sharma A, Kumar A, Singh AK, Kumar KJ, Narasimhan B and Kumar P: Ethnomedicinal uses, phytochemistry, pharmacology, and toxicology of *Ruellia tuberosa* L.: A review. Chem Biodivers 21: e202400292, 2024.
24. Ravi P and Pandey BKS: Phytochemical studies on *Ruellia tuberosa*: A review. Int J Pharm Biol Sci 8: 1190-1195, 2018.
25. Guha S, Talukdar D, Mandal GK, Mukherjee R, Ghosh S, Naskar R, Saha P, Murmu N and Das G: Crude extract of *Ruellia tuberosa* L. flower induces intracellular ROS, promotes DNA damage and apoptosis in triple negative breast cancer cells. J Ethnopharmacol 332: 118389, 2024.
26. Amajida H, Purwoko T and Susilowati A: Antibacterial activity of ethanolic and n-hexane extracts of *Ruellia tuberosa* leaves against *Escherichia coli* and *Bacillus subtilis* bacteria. Biofarmasi J Natural Product Biochem 17: 2580-2550, 2019.
27. Williams and Wilkins Publishers. Bergey's Manual of Systematic Bacteriology. Baltimore, 2: 2001.
28. Clinical and Laboratory Standards Institute (CLSI). Performance standards for antimicrobial susceptibility testing. 32nd edition. CLSI supplement M100. Wayne (PA), Clinical and Laboratory Standards Institute, 2022.
29. Balouiri M, Sadiki M and Ibnsouda SK: Methods for in vitro evaluating antimicrobial activity: A review. J Pharm Anal 6: 71-79, 2016.
30. G S, Pathoor NN, Murthykumar K and Ganesh PS: Targeting *Pseudomonas aeruginosa* PAO1 pathogenicity: The role of *Glycyrrhiza glabra* in inhibiting virulence factors and biofilms. Diagn Microbiol Infect Dis 111: 116674, 2025.
31. Pathoor NN, Ganesh PS, Anshad AR, Gopal RK, Ponmalar EM, Suvaithenamudhan S, Rudrapathy P and Shankar EM: 3-Hydroxybenzoic acid inhibits the virulence attributes and disrupts biofilm production in clinical isolates of *Acinetobacter baumannii*. Eur J Clin Microbiol Infect Dis 44: 653-669, 2025.
32. Girija S, Duraipandiyan V, Kuppusamy PS, Gajendran H and Rajagopal R: Chromatographic characterization and GC-MS evaluation of the bioactive constituents with antimicrobial potential from the pigmented ink of *Loligo duvauceli*. Int Sch Res Notices 2014: 820745, 2014.
33. Surgers L, Boyd A, Girard PM, Arlet G and Decré D: Biofilm formation by ESBL-producing strains of *Escherichia coli* and *Klebsiella pneumoniae*. Int J Med Microbiol 309: 13-18, 2019.
34. Kirana P, Prashantkumar CS, Soundarya R, Shwetha GS, Kalasad MN and Gayathri D: *Tinospora cordifolia's* green synthesis approach: Comparative study on biogenic and chemical synthesis of zinc oxide and zinc sulfide nanoparticles. Materials Int 6: 40, 2024.
35. Buchmann D, Schwabe M, Weiss R, Kuss AW, Schaufler K, Schlüter R, Rödiger S, Guenther S and Schultze N: Natural phenolic compounds as biofilm inhibitors of Multidrug-resistant *Escherichia coli*- the role of similar biological processes despite structural diversity. Front Microbiol 14: 1232039, 2023.
36. Kim Y, Kim S, Cho KH, Lee JH and Lee J: Antibiofilm activities of cinnamaldehyde analogs against uropathogenic *Escherichia coli* and *Staphylococcus aureus*. Int J Mol Sci 23: 7225, 2022.
37. Olszewska MA, Gędas A and Simões M: The effects of eugenol, Trans-Cinnamaldehyde, citronellol, and terpineol on *Escherichia coli* biofilm control as assessed by Culture-dependent and -independent methods. Molecules 25: 2641, 2020.
38. Rony Varughese RM, Pathoor NN, Ranganathan P and Ganesh PS: Efficacy of *Rhamnus frangula* extract against *Acinetobacter baumannii* biofilms: Histopathological evidence from ex vivo goat models. World Acad Sci J 7: 36, 2025.
39. Paula-Ramos L, da Rocha Santos CE, Camargo Reis Mello D, Nishiama Theodoro L, De Oliveira FE, Back Brito GN, Junqueira JC, Jorge AOC and de Oliveira LD: *Klebsiella pneumoniae* planktonic and biofilm reduction by different plant extracts: *In vitro* study. Scientific World Journal 2016: 3521413, 2016.
40. Zubair M: Antimicrobial and Anti-biofilm activities of *Coffea Arabica* L. against the clinical strains isolated from diabetic foot ulcers. Cureus 16: e52539, 2024.
41. Keohane CE, Steele AD, Fetzer C, Khowsathit J, Van Tyne D, Moynié L, Gilmore MS, Karanicolas J, Sieber SA and Wuest WM: Promysalin elicits Species-selective inhibition of *Pseudomonas aeruginosa* by targeting succinate dehydrogenase. J Am Chem Soc 140: 1774-1782, 2018.
42. Mahoney AR, Storek KM and Wuest WM: Structure-based design of promysalin analogues to overcome mechanisms of bacterial resistance. ACS Omega 8: 12558-12564, 2023.
43. Rashiya N, Sangavi J, Padmini N, Langeswaran K, Alagarsamy A, Selvakumar G and Saravanan M: In silico and in vitro analysis of diethyl phthalate as a quorum sensing inhibitor and its antitumor evaluation against MDA-MB-231 cell lines. Mol Divers 30: 761-771, 2026.
44. Rashiya N, Padmini N, Ajilda AAK, Prabakaran P, Durgadevi R, Veera Ravi A, Ghosh S, Sivakumar N and Selvakumar G: Inhibition of biofilm formation and quorum sensing mediated virulence in *Pseudomonas aeruginosa* by marine sponge symbiont *Brevibacterium casei* strain Alu 1. Microb Pathog 150: 104693, 2021.
45. Kim YR and Sang MK: Effects of di-(2-ethylhexyl) phthalate on growth, metabolism, and virulence of the plant pathogenic bacterium *Acidovorax citrulli*. Front Cell Infect Microbiol 13: 1228713, 2023.
46. Louis M, Tahrioui A, Verdon J, David A, Rodrigues S, Barreau M, Manac'h M, Thiroux A, Luton B, Dupont C, *et al*: Effect of phthalates and their substitutes on the physiology of *Pseudomonas aeruginosa*. Microorganisms 10: 1788, 2022.